Supporting Information

Sharma et al. 10.1073/pnas.1220764110

SI Materials and Methods

Bone Marrow Cell Isolation. Pediatric bone marrow (BM) (~1.5–5 mL/donor) was aspirated from the posterior iliac crests, pelves, or femora of male and female spina bifida (SB) or normal donors ($n = 4$ each, 10–17 y of age; normal indicates nondiseased) undergoing orthopedic procedures. Three donor samples from each group were used for multipotent mesenchymal stem cell (MSC) augmentations; one of the three was used for MSC/CD34$^+$ augmentations and an additional sample from each group was used for CD34$^+$ augmentations. Heparinized marrow aspirates were diluted 1:4 with Ca^{2+}- and Mg^{2+}-free Dulbecco's PBS (DPBS) (Invitrogen). Diluted marrow was underlaid with Ficoll-Paque (GE Healthcare) and centrifuged at 800 × *g* for 30 min at 20 °C, after which the mononuclear cell fraction was collected. Target cells were isolated via FACS with CD29-APC (allophycocyanin), CD44-PerCP/Cy5.5 (peridinin chlorophyll protein/cyanine 5.5), CD105-FITC (fluorescein isothiocyanate), CD166-PE (phycoerythrin), CD14-Pacific Blue, CD34-PE/Cy7 (phycoerythrin/cyanine 7), or CD45-APC/Cy7 (allophycocyanin/ cyanine 7) (antibodies from BD Biosciences, BD Pharmingen, Abcam, or eBioscience) to obtain CD29$^+$/CD44$^+$/CD105$^+$/CD166$^+$/CD34$^-$/CD45$^-$/CD14$^-$ MSCs. The MSCs were collected and plated into Mesenchymal Stem Cell Growth Media (MSCGM; Lonza Inc.) for 7–10 d at 37 °C, 5% CO_2 in air. BM was also incubated with the aforementioned anti-CD34 antibody to isolate CD34$^+$ HSPCs via FACS. Isolated MSCs and CD34$^+$ hematopoietic stem/progenitor cells (HSPCs) were used for scaffold seeding in a donor-matched setting, where appropriate. Adult MSCs and CD34$^+$ HSPCs were purchased from Lonza Inc. This study was approved by the Institutional Review Board at the Ann and Robert H. Lurie Children's Hospital of Chicago.

In Vitro Differentiation of Mesenchymal Stem Cells. MSCs underwent coerced terminal differentiation into osteoblasts, adipocytes, and chondrocytes. MSC differentiation into osteoblasts was accomplished using the Mesenchymal Stem Cell Osteogenesis Kit (Millipore). As per manufacturer's instructions, 24-well plates were coated with 500 μL of a 12 μg/mL vitronectin and collagen mixture and allowed to incubate for 16 h at room temperature (RT). Following incubation the solution was removed and washed once with DPBS. MSCs were then plated at a density of 60,000 cells/well in the aforementioned coated plates with 1mL of MSCGM and incubated overnight at 37 °C with 5% CO_2 in air, resulting in wells that were 100% confluent the following day. MSCGM was removed and replaced with osteogenesis induction medium [DMEM-low glucose, 10% (vol/vol) heat-inactivated FBS, 0.1 μM dexamethasone solution, 0.2 mM ascorbic acid 2-phosphate solution, 10 mM glycerol 2-phosphate solution, L-glutamine, and penicillin and streptomycin]. Media was replaced every 2–3 d with fresh osteogenesis induction media for 17 d. MSCs undergoing osteogenic induction were fixed with 70% ethanol for 1 h at RT. After solution removal, wells were washed twice with 500 μL of water and subsequently stained with Alizarin Red S solution (Millipore) at RT for 30 min. The Alizarin Red S solution was removed and the wells were washed four times with water then imaged. Alizarin Red S was used to visualize calcium deposits in osteoblasts. MSC adipogenic differentiation was performed with the plating of 40,000 cells/well in a 24-well plate with 1 mL of MSCGM. Cells were incubated at 37 °C with 5% CO_2 in air for 5 d. Five days postplating, MSCs were 100% confluent and underwent three cycles of an induction/maintenance protocol using Adipogenic Induction Media (AIM; Lonza Inc.). Cells were induced for 3 d with the aforementioned AIM followed by 1–3 d of Adipogenic Maintenance Media (AMM; Lonza Inc.). Following three complete cycles of induction/maintenance, MSCs were cultured in AMM for 7 d, with media replacement every 2–3 d. MSCs were then fixed with 4% paraformaldehyde for 40 min at RT and sequentially washed with DPBS then water. One milliliter of Oil Red O solution (Millipore) was added to wells and allowed to incubate at RT for 50 min. The Oil Red O solution was then removed and wells were washed three times with water and used to identify lipids within differentiated adipocytes. Chondrocyte differentiation of donor MSCs was accomplished using a Mesenchymal Stem Cell Chondrogenesis Differentiation Kit (Invitrogen Cell Culture). Micromass cultures were generated by seeding 5-μL droplets containing 1.6×10^7 viable cells/mL. Micromass cultures were then cultivated for 2 h at 37 °C with 5% CO_2 in air. Following incubation, warmed chondrogenesis differentiation media (1g/L D-glucose, 110 mg/L sodium pyruvate, 5 μg/mL gentamicin, 2 mM L-glutamine, and chondrogenesis supplement) was added. Media was replaced every 2–3 d with fresh chondrogenesis induction medium for 14 d. After 14 d of differentiation with chondrogenesis induction medium, chondrocytes were then fixed with 10% buffered formalin for 2 h at RT. Chondrocytes were then embedded in paraffin using a graded ethanol series and then sectioned onto glass slides. Tissue sections were then deparaffinized and rehydrated with deionized water. Tissue sections were then stained with 1% Alcian blue solution prepared in 0.1 M HCl for 30 min. Following a rinse with deionized water, tissue sections were stained with hematoxylin for 5 min and washed again in deionized water. Samples were then dried and mounted with Permaslip (Alban Scientific Inc.). Sample images (1,024 × 768, bit depth 24) were captured using a Nikon Eclipse 50i microscope (Nikon Inc.) Blue staining indicated synthesis of proteoglycans by chondrocytes. Images were captured using a Leica DM IL light microscope equipped with Hoffman objectives, a Leica DFC295 digital color camera, and Leica software application suite (Leica, Inc.).

In Vitro Proliferation Assay. MSCs were plated in 96-well plates (3,000 cells/well) followed by 18 h of serum deprivation then grown in MSCGM for up to 17 d. At days 1, 3, 5, 7, 10, 12, 14, and 17 media was removed and plates were transferred to −80 °C until a CyQuant cell proliferation assay (Molecular Probes) was performed as previously described (1). Additional MSC-seeded plates provided standards to convert fluorescence intensity values into cell number estimates. A mean estimated cell number was calculated from 12 wells for each sample at each time point. Values were log-transformed for statistical analysis. Fluorescence was measured at 480/520 nm excitation/emission using a Spectramax M5 (Molecular Devices).

Oligonucleotide Genechip Microarray. MSCs from adult (A, $n = 1$ donor), pediatric control (PC, $n = 3$ donors), and pediatric SB (PSB, $n = 3$ donors) groups were used for total RNA isolation using the RNeasy Kit (Qiagen). RNA quality was assessed using the Agilent 2100 Bioanalyzer (Agilent Technologies). Standard cDNA synthesis and subsequent hybridizations to Human Genome U133 Plus 2 microarrays (Affymetrix) were performed by the Center for Applied Genomics at The Hospital for Sick Children, Ontario, ON, Canada per the facility's protocol. Expression data were extracted using the Robust Multiarray Averaging (RMA) method implemented in the BRB Array tool V4.2.1, from the National Center for Biotechnology Information. The probe-set

summaries were computed using a three-step approach that uses a background correction on the Perfect Match data then applies quantile normalization and finally summarizes the probe-set information by using Tukey's median polish algorithm. Differentially expressed genes were identified using a random-variance *t* test that considers within-class variation without assuming equal variance. Genes were considered statistically significant if $P < 0.01$. A global test of whether the expression profiles differed between the classes by permuting the labels of which arrays corresponded to which classes were also used, and for each permutation the *P* values were recomputed and the number of genes significant at the 0.01 level was noted.

MSC Immunophenotyping. Flow cytometric analyses of donor MSCs was performed on a BD LSR Fortessa (Becton Dickinson) preceded by staining with the aforementioned fluorochrome-conjugated antibodies and CD73-PE, CD90-FITC, CD117-FITC, and CD133-PE. Approximately 20,000 gated events were collected for data analysis and plots show labeled and nonlabeled cells at fluorochrome-appropriate settings.

Poly(1,8-octanediol-cocitrate) Scaffold Synthesis. Poly(1,8-octanediol-cocitrate) (POC) scaffold synthesis was accomplished with the addition of equimolar amounts of 1,8 octanediol (Sigma-Aldrich) and citric acid (Sigma-Aldrich) followed by melting at 160 °C with stirring as previously described (2). The temperature of the solution was then slowly reduced to 140 °C for 30 min and subsequently cooled to create a prepolymer. This solution was further dissolved into 100% ethanol, producing a 30% wt/vol solution. This solution was poured into an untreated flat-bottomed glass mold and transferred to a heated oven and underwent polymerization at 55 °C for 7 d. Following postpolymerization, the POC scaffolds were demolded and unreacted monomer was removed by incubation in DMEM (Lonza Inc.) with changes every 6 h within a 24-h period.

POC Scaffold Seeding. Scaffolds were synthesized and mechanical testing was performed as previously described (2). POC scaffolds ($0.50 \times 0.75 \times 0.2$ cm) used for augmentation studies were seeded at 1.5×10^4 MSCs/cm^2 and allowed to grow for 1 wk in vitro before augmentation. CD34$^+$ HSPCs ($1–2 \times 10^5$) were also added to POC or POC/MSC scaffolds and allowed to attach overnight before bladder augmentation procedures in separate studies.

Immunocompromised Rodent Bladder Augmentation Model. Adult athymic female nude rats underwent bladder augmentation as described (3, 4). Intraperitoneal injections of ketamine and xylazine (60 mg/kg and 5 mg/kg, respectively) were used to anesthetize all animals. An injection of the analagesic Buprenex (1 mg/kg) was administered s.c. to diminish any postoperative pain. A 1-cm midline abdominal incision in the vertical plane was created to expose the abdominal wall. This was followed by the physical separation of the abdominal wall, which led to the identification of the urinary bladder. A 50–60% supratrigonal cystectomy was performed from anterior to posterior positions. The cystectomized defect was augmented with the POC/MSC or POC/MSC+CD34$^+$ HSPCs). Unseeded POC scaffolds were used in a previous study and consistently provided results that demonstrated unseeded POC was conducive to high levels of collagen deposition (2). The bladder was sutured shut with 7-0 polyglactin suture in a watertight fashion and was enveloped with omentum in the area containing the POC/cell composites. The abdominal wall was then closed with 5-0 ethibond running suture and the skin closed with 9-mm autoclips. Group-I [A POC/MSC ($n = 3$), A POC/CD34$^+$ ($n = 4$), and A POC/MSC+CD34$^+$ ($n = 6$)]; group-II [PC POC/MSC ($n = 12$), PC POC/CD34$^+$, ($n = 5$), and PC POC/MSC+CD34$^+$ ($n = 3$)]; and group-III [PSB POC/MSC ($n = 11$), PSB POC/CD34$^+$, ($n = 4$), and PSB POC/MSC+CD34$^+$ ($n = 4$)] animals were killed at 4 wk. A POC/MSC ($n = 4$), PC POC/MSC ($n = 25$), and PSB POC/MSC ($n = 24$) animals were killed at 10 wk. A minimum number of three BM donors were used for SB and PSB groups, and one donor was used for the A group for in vivo studies. The differing number of animals used in each study group was dependent on the number of cells isolated from BM samples (where applicable) combined with animal mortality rates.

Histological Analysis of Augmented POC–Tissue Composites. Full-thickness bladder tissue specimens were removed immediately following killing of animals and were fixed in 10% buffered formalin phosphate (Fisher Scientific). Samples were dehydrated through a series of graded ethanol exchanges and embedded in paraffin according to well-established protocols at 4- and 10-wk time points (2). Paraffin-embedded bladder tissue was sectioned onto glass slides (10 μm) using a RM2125 RT microtome (Leica) and was subsequently stained with Masson's trichrome (Sigma-Aldrich). The slides were deparaffinized at 62 °C for 5 min on a hot plate followed by treatment with xylenes, graded ethanol washes, and deionized water. Slides were placed in Bouin's solution for 15 min then rinsed under running tap water. Hematoxylin staining for 5 min followed Bouin's staining and was followed by rinsing and 5 min of staining with Scarlet-Acid Fuchsin. Following a rinse with deionized water, slides were subjected to a mixture of phosphotungstic acid/phosphomolybdic acid stain, followed by Aniline Blue staining. Finally, a solution of 1% acetic acid was used as a wash. Slides were then placed in 95–100% ethanol and rinsed in xylene. After drying, a coverslip was placed over the tissue and secured with two or three drops of Permaslip (Alban Scientific Inc.).

Quantitative Evaluation of Histological Stained POC–Tissue Composites. Adult athymic female nude rats (~200–250 g ; NCI) underwent bladder augmentation as described (2). The cystectomized defect was augmented with POC/MSC, POC/CD34$^+$ HSPCs, POC/MSC+CD34$^+$ HSPC, or seeded POC scaffolds. Groups I–III described above were killed at 4 wk. A POC/MSC, PC POC/MSC, and PSB POC/MSC animals were killed at 10 wk. Full-thickness bladder tissue specimens were removed at their respective time points and underwent Masson's trichrome (Sigma-Aldrich) staining and were evaluated for muscle and collagen content by an established protocol (2).

Explanted bladder tissue/scaffolds that underwent Masson's trichrome staining were evaluated for muscle and collagen content. Muscle-to-collagen ratios were digitally quantified using a Nikon Eclipse 50i microscope (Nikon Inc.) and Spot Advanced Imaging software (Diagnostic Instruments). Sample images ($1,600 \times 1,200$ pixels, bit depth 24) were opened with Adobe Photoshop CS3 (Adobe Systems Inc.). The contrast of red pixels from blue pixels was enhanced by a twofold elevation of magenta levels followed by a twofold depression of cyan levels in the red and magenta spectra. This contrast was further improved by a twofold elevation of cyan levels followed by a twofold depression of magenta levels in the cyan and blue spectra. The color-range selection tool with a fuzziness level of 115% was then used to digitally select the red or blue pixels of the entire image. Selected pixels were subsequently quantified using the image histogram tool and a muscle-to-collagen ratio was calculated from these values. In cases in which urothelial cells, red blood cells, or debris were present, images were edited to remove these structures to preserve a more accurate representation of the muscle-to-collagen ratio from the red-to-blue ratio. Areas of regenerated tissue were subjected to an average of 12 random microscopic fields to determine muscle-to-collagen ratios as previously described (2). All data are shown as percent muscle means ± SE. All animal procedures were performed in accordance with guidelines set forth and approved by the Ann

and Robert H. Lurie Children's Research Center Institutional Animal Care and Use Committee.

Immunofluorescent and Quantitative Analysis of Augmented Tissues. Following the dehydration, embedding, and deparaffinization process as previously described, tissue samples were subjected to immunofluorescent staining. Briefly, slides were subjected to antigen retrieval consisting of 15 min of boiling in citrate buffer [0.01 M citrate solution (pH 6.0) with 0.05% Tween-20] and then cooled to RT for ~30 min. Staining consisted of a blocking step for 15 min in BSA (5 mg/mL) followed by a 40-min incubation at RT with the primary antibody. After washing with DPBS, slides were incubated for 30 min with a secondary antibody and eventually rinsed with DPBS and air-dried. Slides were mounted with Vectashield (Vector Laboratories). Primary antibodies used in this study were directed against epitopes for markers of bladder smooth muscle cells using antibodies against smooth muscle γ-actin (Millipore), calponin, or caldesmon. K_i-67, human reactive γ-tubulin and elastin, CD31, αvβ3, and FGF9 were also used (all from Santa Cruz Biotechnology Inc.) and Wnt10a and vWF (Abcam) in conjunction with either an Alexa Red 555 or FITC conjugated secondary antibody (Molecular Probes) following established protocols (2). The antineuronal antibodies βIII tubulin and synaptophysin (Covance Inc. and Santa Cruz Biotechnology Inc., respectively) were used to determine the extent of peripheral nerve growth in areas of regenerated bladder. Primary antibodies were used at dilutions from 1:100–1:250. Species-specific secondary antibodies were used at a 1:400 dilution. Immunofluorescence quantification was carried out using a Nikon Eclipse 50i microscope (Nikon Inc.) and Spot Advanced Imaging software (Diagnostic Instruments). The number of K_i-67$^+$ cells was determined by manual counting through the utilization of the eraser tool within Adobe Photoshop to mark colored cells. Fluorescent images (1,600 × 2,000 pixels, bit depth 24) were opened with Adobe Photoshop CS3 (Adobe Systems Inc.). All samples were additionally stained with DAPI to identify cells by nuclei visualization.

Quantification of in Vivo Vessel Formation. Trichrome sample images (1,600 × 2,000 pixels, bit depth 24) were opened with Adobe Photoshop CS3 (Adobe Systems Inc.) and were initially characterized using a Nikon Eclipse 50i microscope (Nikon Inc.) equipped with Spot Advanced Imaging software (Diagnostic Instruments). Vessel numbers were quantified using the pen tool based on nine images per graft in both native and regenerated areas. Individual vessels were selected manually and subsequently quantified using the image histogram tool to acquire pixel density for each vessel. Data are represented as mean number of vessels per square millimeter and mean percent vasculature (means ± SE).

Laser-Capture Microdissection and Quantitative PCR. Cell/scaffold specimens were isolated immediately after animals were killed and were fixed in 10% buffered formalin phosphate (Fisher Scientific). The tissue was dehydrated through a series of graded ethanol exchanges followed by paraffin washes and placed into molds. Samples were sectioned at a thickness of 10 μm using a RM2125 RT Microtome (Leica) onto membrane slides (Zeiss) and subjected to staining with Wnt10a (Abcam). Tissue-containing slides were blocked for 15 min in BSA (5 mg/mL) followed by a 30-min incubation at RT with Wnt10a antibody at a 1:100 dilution. After washing with DPBS, slides were incubated for 30 min with an Alexa Red 568 secondary antibody at a 1:400 dilution. Slides were then rinsed with DPBS and allowed to dry. Specific sections of the regenerated urothelium positive for Wnt10a expression were removed by laser-capture microdissection on a Zeiss PALM Microdissection System. Samples were collected in an AdhesiveCap (Zeiss) and then immediately taken for RNA extraction using a NucleoSpin FFPE RNA Kit (Macherey-Nagel) per the manufacturer's instructions. RNA was subjected to PCR assays using the WNT Signaling Pathway RT^2 PCR Array (Qiagen) according to the manufacturer's protocol. Following analysis of PCR data, tissue sections from A, PC, and PSB samples containing either MSCs, CD34$^+$ HSPCs, or MSC/CD34$^+$ HSPCs were stained with antibodies against the WNT protein family members TCF3/4, Axin 1, CTNNB1, and FZD5 (Abcam; Fig. S6*B*) to determine the presence of these proteins in urothelium regeneration.

Statistical Analysis. Differences between bladder augmentation groups were determined using ANOVA, with the Tukey–Kramer adjustment for multiple comparisons. Paired *t* test was used for comparison of native and regenerated tissue within each group. In vitro proliferation data were analyzed using a linear mixed polynomial model with a random intercept, after logarithm transformation of repeated measurements; pairwise comparisons were conducted using the Tukey–Kramer method. $P < 0.05$ was considered statistically significant. Analyses were performed using SAS 9.2 software (SAS Institute). The proliferation data plot was generated using R software (R Foundation for Statistical Computing, www.r-project.org).

1. Biswas S, et al. (2010) Hypoxia inducible microRNA 210 attenuates keratinocyte proliferation and impairs closure in a murine model of ischemic wounds. *Proc Natl Acad Sci USA* 107(15):6976–6981.
2. Sharma AK, et al. (2010) Urinary bladder smooth muscle regeneration utilizing bone marrow derived mesenchymal stem cell seeded elastomeric poly(1,8-octanediol-co-citrate) based thin films. *Biomaterials* 31(24):6207–6217.
3. Aslan A, Akkaya B, Karagüzel G, Karpuzoglu G, Melikoglu M (2004) Bladder augmentation with an omental pedicled gastric seromuscular flap without the necessity of gastric resection. *Urol Res* 32(4):298–303.
4. Caione P, Capozza N, Zavaglia D, Palombaro G, Boldrini R (2006) In vivo bladder regeneration using small intestinal submucosa: Experimental study. *Pediatr Surg Int* 22(7):593–599.

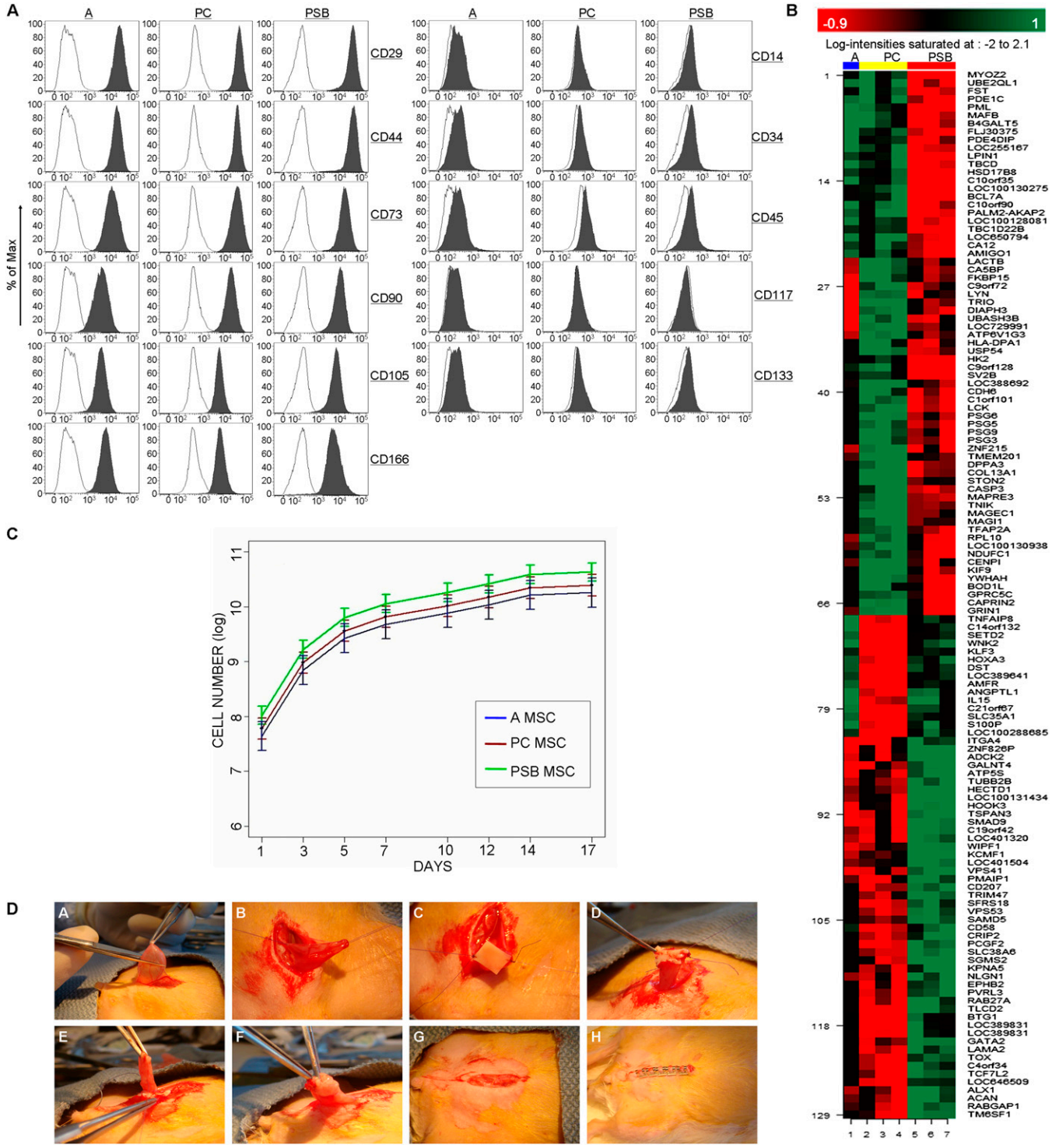

Fig. S1. (*A*) MSC immunophenotyping. Immunophenotyping data of donor MSCs revealed the expression of surface markers CD29, CD44, CD73, CD90, CD105, and CD166. The expression of the hematopoietic cell lineage markers CD14, CD34, CD45, CD117, and CD133 were absent from these donor samples. Data are representative of multiple donor samples in the case of PC and PSB samples. (*B*) Microarray analysis of donor MSCs. Microarray analyses revealed differential expression of 129 unique genes ($P < 0.01$) between PSB and PC samples. Data are representative of multiple donor samples in the case of PC and PSB groups (A, $n = 1$ donor; PC, $n = 3$ donors; PSB, $n = 3$ donors; $P < 0.01$). (*C*) In vitro proliferation analysis of donor MSCs. MSCs isolated from each donor group (A, PC, or PSB) demonstrated a rapid growth phase from days 1–5 of culture followed by a gradual decrease in growth over the remaining duration of the experiment. However, there were no significant differences with regard to proliferative capacity between donor groups at any given time point. In vitro proliferation data for A, PC, and PSB MSCs were analyzed using a linear mixed polynomial model with a random intercept, after logarithm transformation of repeated measurements. Pairwise comparisons were conducted using the Tukey–Kramer method. Adjusted *P* values of <0.05 were considered significant (SAS 9.2 software; SAS Institute). The data plot was generated using R Software (R Foundation for Statistical Computing, www.r-project.org). (*D*) Bladder augmentation procedure. A nude rat bladder augmentation animal model was used as previously described (2, 3). (A) Following preoperative procedures and anesthetization, a ~50% bladder cystectomy was performed with removal of the bladder dome. (B) Stay sutures were put into place at the 9:00 and 3:00 positions to stabilize and

Legend continued on following page

orient the bladder. (C–D) The bladder defect was capped with POC ($^{+/-}$ cells) followed by suturing along the perimeter of the POC with attachment to the freshly excised underlying bladder tissue in a watertight fashion. (E–F) Rat omentum was gently draped over surgically repaired bladder and subsequently sutured in place. (G–H) The abdominal wall was then closed with a running suture and the skin was closed with 9-mm autoclips.

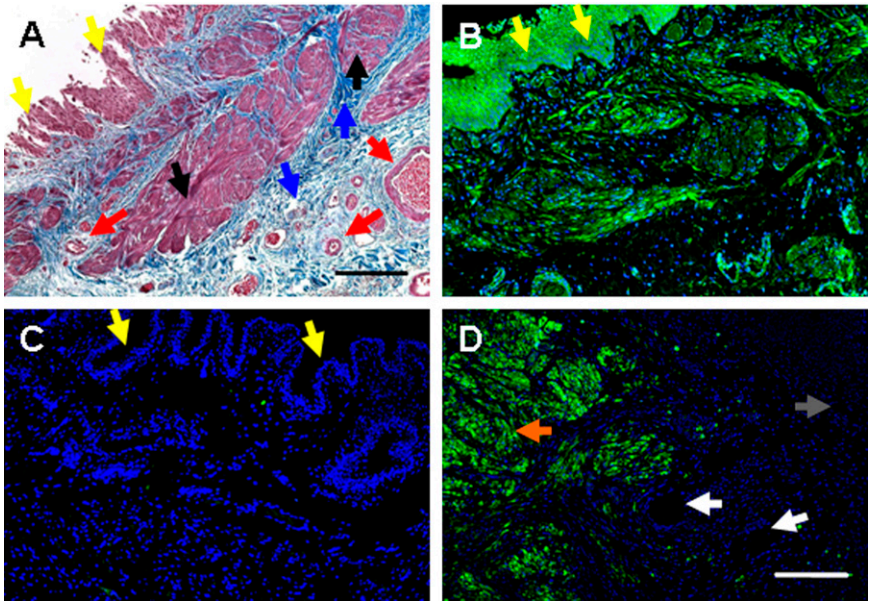

Fig. S2. Control experiments. (*A*) Human bladder tissue stained with Masson's trichrome demonstrated normal trilayer bladder architecture and was used as a visual comparison with POC/cell-augmented scaffolds within the context of this study. Yellow arrows indicate the watertight urothelial cell layer (located on the luminal side of the bladder) and black arrows depict highly organized muscle fascicles. Blue arrows indicate areas of collagen and red arrows denote blood vessels. The typical distribution of muscle to collagen found in the bladder is ~1:1. (4). (*B*) To demonstrate the specificity of the γ-tubulin monoclonal antibody (green) to human bladder tissue, the tissue underwent staining and all aspects of the bladder tissue including muscle and urothelium (yellow arrows) stained in a positive manner. (*C*) Rat bladder tissue was also stained with the γ-tubulin antibody with no apparent positive signal present (yellow arrows depict urothelium). This image is representative of eight different rat bladders stained with γ-tubulin. (*D*) A human (MSCs)/rat hybrid bladder tissue was stained with the γ-tubulin antibody and clearly demonstrates the demarcation between human and rat tissue. Suture artifacts (holes, indicated by white arrows) and the POC scaffold itself were also used for orientation purposes. It has also been previously demonstrated that the γ-tubulin antibody is nonreactive with rat bladder tissue (2). The orange arrow indicates human tissue and the gray arrow indicates rat tissue. Images in *B–D* are counterstained with DAPI (blue) to visualize cell nuclei. (Scale bars, 200 μm.)

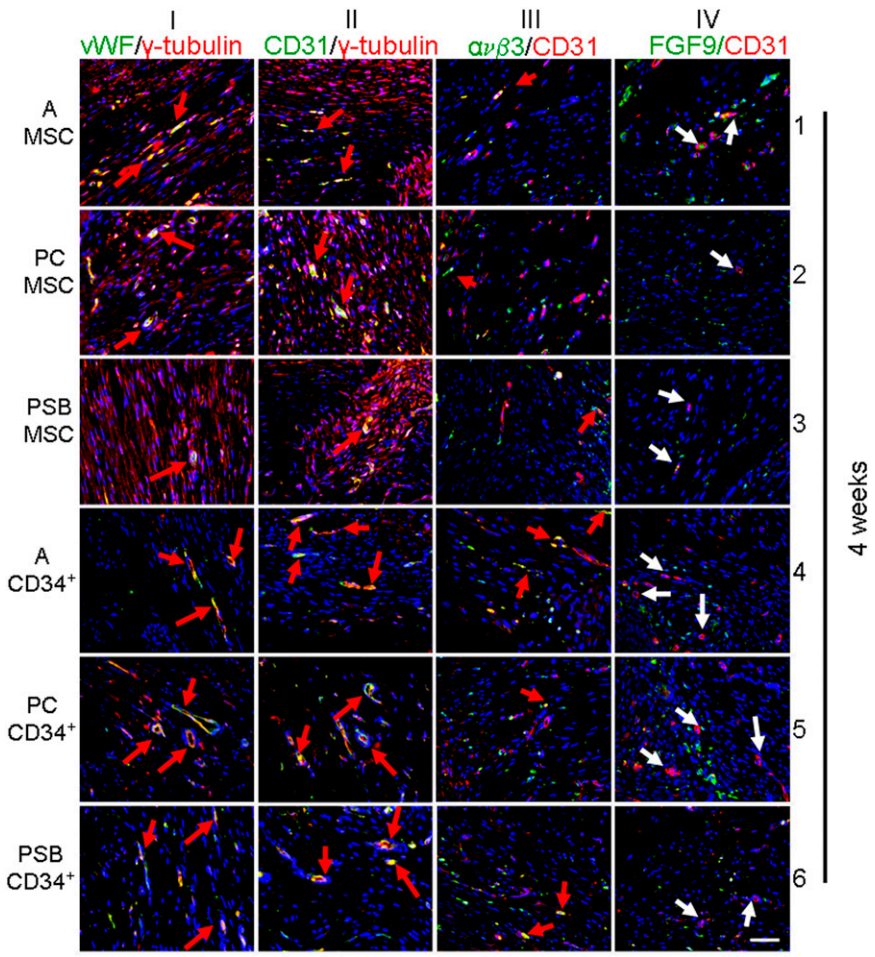

Fig. S3. Tissue vascularization. Achieving adequate vascularization throughout engrafted tissue has been a major obstacle in tissue regeneration studies. This is particularly true at the core of grafts where gas/nutrient exchange is especially poor. Independent seeding of MSCs or $CD34^+$ HSPCs to scaffolds provided an increase in vasculature compared with unseeded scaffolds (at 4 wk), although the addition of $CD34^+$ HSPCs provided an even greater degree of vasculature per area (vessels per square millimeter) and overall percent vasculature. The best results with regard to vasculature growth were demonstrated with MSC/$CD34^+$ HSPCs-seeded scaffolds (Fig. 3 *B* and *C*, respectively). Quantitative data were substantiated by coimmunostaining with established vascular endothelial cell markers (vWF and CD31) along with human reactive γ-tubulin. $vWF^+/\gamma\text{-tubulin}^+$ vasculature in all donor cell-seeded samples is indicated by yellow-orange costaining (column I). This was verified with a second vascular endothelial cell marker, CD31 (column II). Under both circumstances, coimmunostaining with γ-tubulin indicated that the vasculature contained human cells. The extent of FGF9 staining was greatly diminished in MSC- or $CD34^+$ HSPC-seeded scaffolds, which is in complete contrast to MSC/$CD34^+$ HSPC-seeded scaffolds, which demonstrated vigorous FGF9 staining adjacent to muscle bundles and vasculature (1). Red and white arrows denote vasculature. Images are counterstained with DAPI (blue) to visualize cell nuclei. (Scale bar, 50 μm.)

1. Frontini MJ, et al. (2011) Fibroblast growth factor 9 delivery during angiogenesis produces durable, vasoresponsive microvessels wrapped by smooth muscle cells. *Nat Biotechnol* 29(5): 421–427.

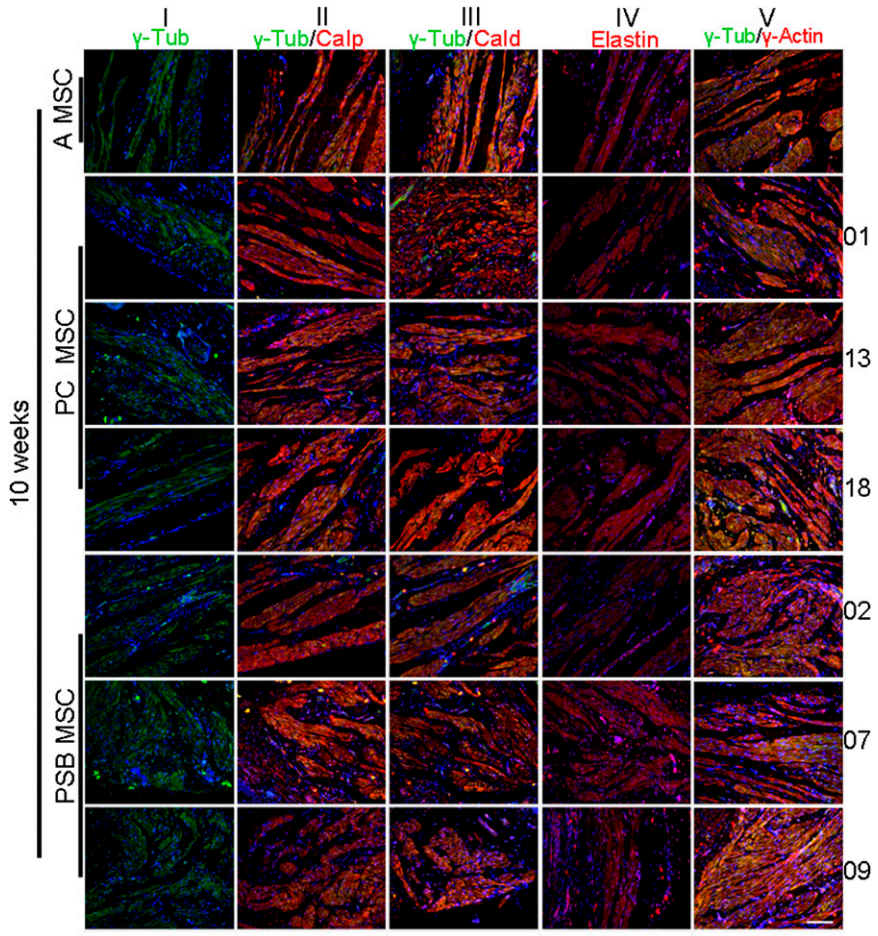

Fig. S4. Regenerated tissue in MSC grafts. The structural protein γ-tubulin organizes microtubules within the nucleus and cytoplasm and is essential during cell division. Column I represents images of A, PC, and PSB samples expressing γ-tubulin (green) within the regenerated area of POC/MSC-seeded samples. The homogenous distribution of human-reactive γ-tubulin indicates that implanted human MSCs were retained within the graft 10 wk post-augmentation with similar expression levels across groups based on subjective evaluation. Hence, the expression of γ-tubulin was not altered by the SB disease process. Similarly, calponin (a marker of smooth muscle cell differentiation and regulator of smooth muscle contraction) and caldesmon (expressed on thin filaments of smooth muscle cells) when used in conjunction with γ-tubulin (columns II and III, respectively) again stain in a manner appearing consistent within the tissue demonstrating colocalized expression (orange in color) of both markers. This distribution and colocalization is also evident using the human-specific elastin (a key protein necessary in bladder contraction) antibody and smooth muscle I-actin antibody paired with γ-tubulin. Cells appear red and orange in color (columns IV and V, respectively). All samples demonstrated the morphological appearance of smooth muscle fascicles at 10 wk postaugmentation. Blue, DAPI. (Scale bars, 100 μm.)

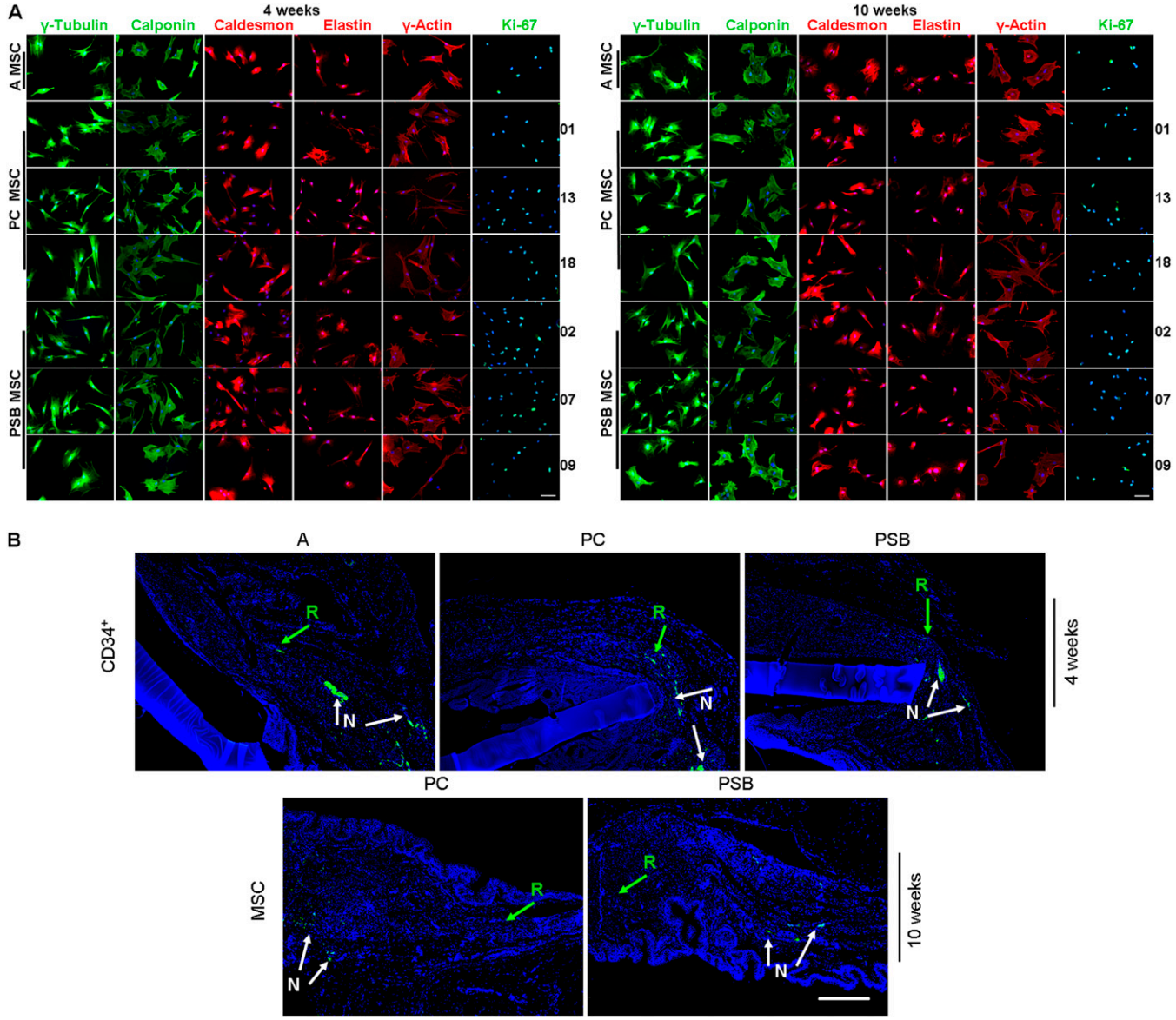

Fig. S5. (*A*) In vitro MSC culturing. Several contractile proteins found in bladder smooth muscle cells are pivotal for overall, coordinated bladder contraction, and the expression of these contractile proteins was also apparent in MSCs in vitro. Immunostaining with a battery of antibodies against these proteins demonstrated strong expression at 4 and 10 wk of culture among A, PC (donors 01, 13, 18), and PSB (donors 02, 07, 09) groups. Cell proliferation as subjectively measured by K_i-67 expression also demonstrated high proliferative capacity of these cells even after 10 wk in culture. K_i-67 images are counterstained with DAPI (blue) to visualize cell nuclei as indicated by a teal-colored colocalization. (Scale bar, 50 μm.) (*B*) The effect of MSC/CD34$^+$ HSPCs on bladder peripheral nerve growth. Micturition cycles of the bladder are in part governed by action potentials conducted through peripheral nerves encompassing the entirety of the bladder. The process of bladder cystectomy destroys these conduits, thus severely hampering the degree of bladder contractility. Currently, bladder peripheral nerve regeneration has not been conclusively demonstrated. The augmentation of CD34$^+$ HSPC-seeded POC scaffolds provides minor peripheral nerve regeneration in A, PC, and PSB donor samples at 4 wk postaugmentation. Neuronal-specific βIII tubulin staining (green) demonstrates minimal peripheral nerve staining at the border of areas of regenerated tissue (denoted as a green R) and areas of native tissue (denoted by a white N) (row 1). MSC-seeded POC scaffolds at 10 wk postaugmentation demonstrated a lack of peripheral nerves in the regenerated area as demonstrated by βIII tubulin staining for PC and PSB samples (green) (row 2). Areas of regeneration were determined by POC scaffold boundaries and locations of suture markings. Images are representative of multiple donor groups (in the case of PC and PSB) and multiple animals. Images are counterstained with DAPI (blue) to visualize cell nuclei. (Scale bar, 500 μm.)

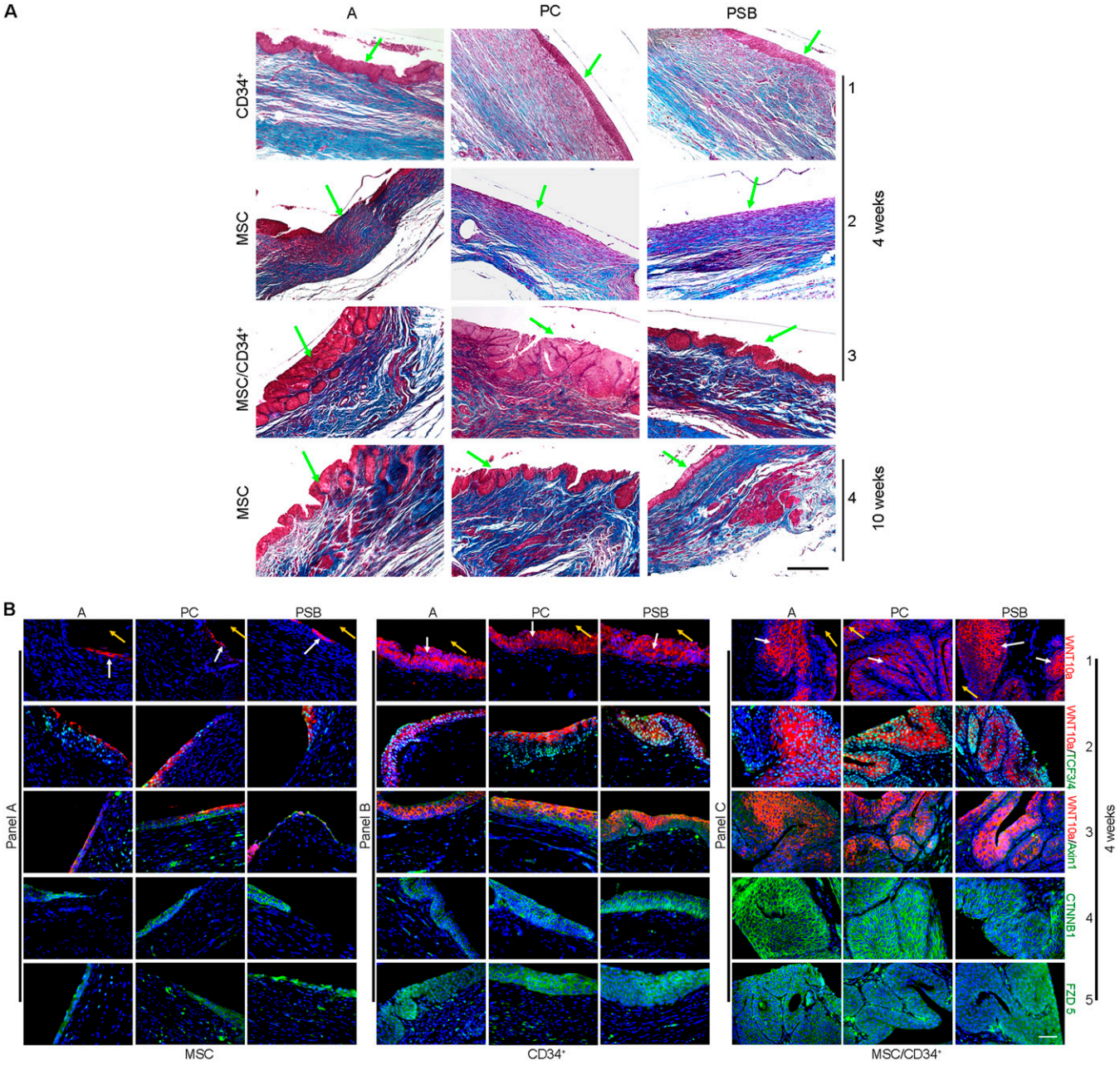

Fig. S6. (*A*) Urothelium regeneration of explanted POC/cell composites. One physiological aspect of the urothelium is to provide an effective, impermeable barrier against urine. This is accomplished in part by the expression and regulation of intercellular urothelial proteins in the form of tight junctions. Hence, the lack of a properly organized urothelium leads to an ineffective barrier against urine, which facilitates leakage into the abdominopelvic cavity, causing peritonitis and subsequent infection. Images in row 1 depict explanted CD34$^+$ HSPC scaffolds 4 wk postaugmentation that display a thin layer of native urothelium in an area of regeneration. The converse is demonstrated in MSC-seeded scaffolds (row 2) at the same time point, in which a suboptimal and tenuous urothelial layer is present. Note the lack of structural organization corroborated quantitatively by poor muscle/collagen ratios in both cell types evident in all donor groups. The combination of MSC/CD34$^+$ HSPCs at 4 wk postaugmentation provides the most robust urothelial growth output of native urothelium in regenerated areas (row 3). The degree of urothelium thickness is similar to that of normal bladder tissue (Fig. S2*A*) as well as MSC-seeded scaffolds 10 wk postaugmentation across all donor groups (row 4). Bladder architecture appears normal including defined muscle fascicles with an approximate 1:1 ratio of muscle/collagen. Data suggests that the addition of CD34$^+$ HSPCs to MSC-containing grafts contributes to the heightened regenerative capacity of the urothelium. Samples were stained with Masson's trichrome. Green arrows indicate urothelium. Images are representative of multiple animal bladder samples. (Scale bar, 250 μm.) (*B*) Wnt proteins are up-regulated in regenerating urothelium. Members of the Wnt family of proteins have been associated with pleiotropic effects in a variety of biological systems within differing organisms. These highly conserved proteins have also been implicated in stem cell self-renewal-affiliated tissue regeneration (1–4). Within the context of this experiment, we demonstrate that specific members of the Wnt family contribute to rapid and robust native urothelial regeneration in conjunction with seeded BM cells. MSC-seeded POC scaffolds (Panel A) demonstrate a mild regenerative response of native urothelium as demonstrated by Wnt10a expression (red in color demarcated by white arrows, row 1). Subsequent costaining of Wnt10a with Wnt family members TCF3/4 and Axin1 (rows 2 and 3, respectively; orange in color) demonstrated expression within the regenerating portion of the urothelium of all donor samples. Native urothelium directly adjacent to regenerating urothelium was devoid of Wnt10a based on antibody staining. CTNNB1 and FZD5 (a receptor for Wnt ligands) were also detected on analyzed urothelium (rows 4 and 5, respectively). The addition of CD34$^+$ HSPCs resulted in a greater degree of Wnt10a-based urothelium regeneration, although urothelium was still tenuous in nature (row 1, Panel B). Staining with the aforementioned Wnt

Legend continued on following page

family members found in Panel A demonstrated similar expression and distribution of these proteins within the urothelium. The combination of MSC/CD34$^+$ HSPC-seeded POC scaffolds (Panel C) with analogous samples demonstrate optimal urothelium growth as early as 4 wk postaugmentation in regenerating bladder tissue accompanied by strong up-regulation of Wnt10a expression (row 1). The early onset of the protective urothelial lining in the MSC/CD34$^+$ HSPC groups may have also provided an environment conducive to the superior muscle and vascular growth as demonstrated in Figs. 2 and 3. Further staining of tissues with antibodies directed against Wnt proteins revealed multiple pathway regulators found downstream of Wnt ligand signaling (rows 2–5). The choice to select the aforementioned protein partners of Wnt10a [TCF3/4, Axin1, CTNNB1 (β-catenin), and the FZD5] was based on laser-capture microdissection of urothelium in MSC-, CD34$^+$-, or MSC/CD34$^+$-seeded scaffolds that were initially Wnt10a$^+$ by immunostaining. This was followed by quantitative PCR against a Wnt signaling family-based PCR array (Qiagen). Several other Wnt family members were found to be up-regulated in the urothelium by PCR, including CCND2, rac1, SFRP2, PORCN, and BTRC. Yellow arrows indicate the lumen of the bladder. All samples are 4 wk postaugmentation. (Scale bar, 50 μm.)

1. Kalani MY, et al. (2008) Wnt-mediated self-renewal of neural stem/progenitor cells. *Proc Natl Acad Sci USA* 105(44):16970–16975.
2. Reya T, et al. (2003) A role for Wnt signalling in self-renewal of haematopoietic stem cells. *Nature* 423(6938):409–414.
3. Shin K, et al. (2011) Hedgehog/Wnt feedback supports regenerative proliferation of epithelial stem cells in bladder. *Nature* 472(7341):110–114.
4. Miyoshi H, Ajima R, Luo CT, Yamaguchi TP, Stappenbeck TS (2012) Wnt5a potentiates TGF-β signaling to promote colonic crypt regeneration after tissue injury. *Science* 338(6103): 108–113.

Table S1. Quantification of in vitro trilineage cellular differentiation of MSC donor groups

Group and donor	Osteoblast staining Alizarin Red S (% red)	Adipocyte staining Oil Red O (% red)	Chondrocyte staining Alcian blue (% blue)
A MSC	14.5 ± 1.3	38.2 ± 3.9	75.2 ± 1.5
PC MSC			
01	15.8 ± 1.5	34.9 ± 1.9	74.4 ± 1.4
13	14.4 ± 1.7	37.7 ± 2.3	74.8 ± 1.4
18	15.6 ± 2.3	39.2 ± 4.6	72.0 ± 0.9
PSB MSC			
02	26.7 ± 2.3	38.4 ± 2.8	74.0 ± 1.5
07	16.7 ± 2.1	35.1 ± 1.9	74.8 ± 2.7
09	14.6 ± 1.1	43.3 ± 3.6	75.3 ± 1.2

The multipotential nature of donor MSCs was evaluated in vitro from all MSC donor groups as demonstrated in Fig.1 *B–D*. Subsequent cellular quantification of these groups revealed similar levels of differentiation across donor groups for all lineages. Osteoblast and adipocyte stained (n = 4 images each) or chondrocyte stained (representing two micromasses; n = 10 images total) images were quantified for each donor sample. The degree of staining was quantified for each image by determining pixel counts. Red pixels indicated staining by Alizarin Red (osteoblasts) S or Oil Red O (adipocytes) and blue pixels indicated staining by Alcian blue (chondrocytes). Osteoblast and adipocyte percentages were determined by the formula (red pixels/total pixels) × 100. Chondrocyte percentages were determined by the formula (blue pixels/total pixels) × 100. Data are shown as means ± SE.

Table S2. Gene ontology (GO) analysis between PC and PSB MSCs

GO ID	GO term	Observed in selected subset	Expected in selected subset	Observed/ expected
Cellular component				
GO:0005604	Basement membrane	5	0.82	6.08
GO:0044420	Extracellular matrix part	7	1.37	5.11
GO:0005813	Centrosome	8	1.95	4.10
GO:0005874	Microtubule	8	2.39	3.35
GO:0005578	Proteinaceous extracellular matrix	8	3.05	2.63
GO:0005815	Microtubule organizing center	8	3.13	2.55
GO:0016604	Nuclear body	5	2.00	2.49
GO:0044456	synapse part	7	3.09	2.26
Molecular function				
GO:0015631	Tubulin binding	6	1.06	5.64
GO:0005529	Sugar binding	5	1.46	3.42
GO:0004842	Ubiquitin-protein ligase activity	5	1.79	2.80
GO:0005096	Gtpase activator activity	6	2.23	2.69
GO:0016881	Acid-amino acid ligase activity	7	2.69	2.60
GO:0019787	Small conjugating protein ligase activity	5	1.94	2.58
GO:0030246	Carbohydrate binding	7	2.95	2.37
GO:0016879	Ligase activity, forming carbon–nitrogen bonds	7	3.04	2.30
GO:0005083	Small gtpase regulator activity	5	2.26	2.22
GO:0003779	Actin binding	5	2.47	2.02
Biological process				
GO:0050773	Regulation of dendrite development	5	0.27	18.24
GO:0016358	Dendrite development	5	0.56	8.85
GO:0008629	Induction of apoptosis by intracellular signals	5	0.71	7.00
GO:0050769	Positive regulation of neurogenesis	5	0.73	6.84
GO:0010720	Positive regulation of cell development	6	0.95	6.33
GO:0010769	Regulation of cell morphogenesis involved in differentiation	7	1.24	5.65
GO:0022604	Regulation of cell morphogenesis	7	1.25	5.62
GO:0048705	Skeletal system morphogenesis	7	1.25	5.58
GO:0002429	Immune response-activating cell surface receptor signaling pathway	6	1.08	5.56
GO:0010975	Regulation of neuron projection development	7	1.26	5.54
GO:0002768	Immune response-regulating cell surface receptor signaling pathway	6	1.11	5.39
GO:0045216	Cell–cell junction organization	6	1.20	5.01
GO:0050851	Antigen receptor-mediated signaling pathway	5	1.01	4.97
GO:0031344	Regulation of cell projection organization	7	1.51	4.63
GO:0045664	Regulation of neuron differentiation	9	2.00	4.49
GO:0050870	Positive regulation of T-cell activation	7	1.58	4.43
GO:0050863	Regulation of T-cell activation	9	2.11	4.26
GO:0051640	Organelle localization	5	1.18	4.24
GO:0048562	Embryonic organ morphogenesis	7	1.66	4.21
GO:0051251	Positive regulation of lymphocyte activation	9	2.17	4.15
GO:0050804	Regulation of synaptic transmission	5	1.24	4.04
GO:0002696	Positive regulation of leukocyte activation	9	2.28	3.94
GO:0050867	Positive regulation of cell activation	9	2.33	3.87
GO:0030217	T-cell differentiation	5	1.35	3.71
GO:0051969	Regulation of transmission of nerve impulse	5	1.35	3.69
GO:0030098	Lymphocyte differentiation	7	1.93	3.63
GO:0034330	Cell junction organization	8	2.27	3.53
GO:0032844	Regulation of homeostatic process	5	1.47	3.40
GO:0046651	Lymphocyte proliferation	5	1.48	3.38
GO:0031644	Regulation of neurological system process	5	1.50	3.34
GO:0032943	Mononuclear cell proliferation	5	1.50	3.32
GO:0006457	Protein folding	7	2.14	3.27
GO:0070661	Leukocyte proliferation	5	1.54	3.25
GO:0048568	Embryonic organ development	8	2.55	3.14
GO:0072507	Divalent inorganic cation homeostasis	7	2.32	3.02
GO:0072503	Cellular divalent inorganic cation homeostasis	6	2.23	2.68
GO:0046879	Hormone secretion	5	1.87	2.67
GO:0051130	Positive regulation of cellular component organization	7	2.72	2.58

Table S2. Cont.

GO ID	GO term	Observed in selected subset	Expected in selected subset	Observed/ expected
GO:0006605	Protein targeting	7	2.72	2.58
GO:0001501	Skeletal system development	9	3.52	2.55
GO:0009914	Hormone transport	5	1.97	2.54
GO:0002521	Leukocyte differentiation	7	2.78	2.51
GO:0006887	Exocytosis	5	2.06	2.43
GO:0071845	Cellular component disassembly at cellular level	5	2.14	2.34
GO:0022411	Cellular component disassembly	5	2.17	2.31
GO:0055074	Calcium ion homeostasis	5	2.18	2.30
GO:0045596	Negative regulation of cell differentiation	6	2.64	2.27
GO:0010817	Regulation of hormone levels	9	3.97	2.27
GO:0007548	Sex differentiation	5	2.20	2.27
GO:0055080	Cation homeostasis	8	3.55	2.25
GO:0030003	Cellular cation homeostasis	7	3.16	2.22
GO:0043009	Chordate embryonic development	9	4.13	2.18
GO:0009792	Embryo development ending in birth or egg hatching	9	4.20	2.15
GO:0055065	Metal ion homeostasis	6	2.87	2.09
GO:0051093	Negative regulation of developmental process	7	3.41	2.05
GO:0003002	Regionalization	6	2.92	2.05
GO:0045944	Positive regulation of transcription from RNA polymerase II promoter	8	3.95	2.03

The classification of microarray data comparing PC and PSB gene expression patterns yielded data distributed into three distinct GO categories (cellular, molecular, and biological components). Data were derived based on the number of observed gene changes compared against the number of expected occurrences. The term "observed" is defined by a cutoff *P* value of <0.01, which categorized 194 genes that were considered significant within this experiment. The term "expected" is defined as the average number of genes that would be predicted to fall into a specific Gene Ontology category of randomly selected genes from the aforementioned analysis. Only GO classes and parent classes with a minimum of five observations within each selected subset and with an observed vs. expected ratio of at least 2 are shown.

Table S3. Quantification of blood vessels in regenerated tissue containing cells of human origin at 4 wk

	γ-tubulin$^+$/CD31$^+$ vessels (%)		
Group	MSC	CD34$^+$	MSC/CD34$^+$
A	56.8 ± 2.3	54.1 ± 3.6	62.3 ± 3.8
PC	52.3 ± 4.4	51.4 ± 4.3	61.5 ± 4.0
PSB	58.5 ± 6.8	52.3 ± 4.3	64.7 ± 4.3

To determine the cellular makeup of new blood vessels in areas of bladder tissue regeneration, tissue samples from all donor samples containing either MSCs, CD34$^+$ HSPCs, or MSC/CD34$^+$ HSPCs were quantified for γ-tubulin$^+$/CD31$^+$ blood vessels 4 wk postaugmentation. Data revealed overlapping levels of γ-tubulin$^+$/CD31$^+$ blood vessels in each cell type used with a slight increase in the levels found within MSC/CD34$^+$ groups. Data suggest varying degrees of involvement of MSCs and CD34$^+$ HSPCs in new vessel formation. Data are represented as the number of total γ-tubulin$^+$/CD31$^+$ vessels/total number of CD31$^+$ vessels. Data were obtained by manual counting of positively stained vessels.

Table S4. Vessel quantification for native and regenerated bladder tissue

		Group, 4 wk									Group, 10 wk		
		A			PC			PSB			A	PC	PSB
Bladder tissue	Unseeded	MSC	$CD34^+$	MSC/ $CD34^+$	MSC	$CD34^+$	MSC/ $CD34^+$	MSC	$CD34^+$	MSC/ $CD34^+$	MSC	MSC	MSC
Native tissue (vessels/mm^2)	39.7 ± 5.5	44.8 ± 5.0	34.8 ± 5.1	41.1 ± 5.5	35.5 ± 2.8	35.3 ± 6.0	37.5 ± 3.0	37.2 ± 3.8	34.4 ± 1.8	45.3 ± 5.4	40.3 ± 5.6	41.5 ± 3.5	44.2 ± 2.5
Regenerated tissue (vessels/mm^2)	63.8 ± 5.4	83.4 ± 15.8***	147.8 ± 11.0*	230.9 ± 11.4	85.4 ± 4.4***	184.4 ± 9.3***	269.2 ± 19.8	88.7 ± 3.4***	170.4 ± 7.8***	255.7 ± 10.2	82.7 ± 5.5	83.4 ± 3.6	77.1 ± 3.9

Data presented in Fig. 3*B* display the striking differences in vessel number that is dependent on cell type used for augmentation as depicted in graphical form. Native tissue among all donor groups and cell types across both time points demonstrate similar numbers of vessels including unseeded POC scaffolds used for augmentation. Adult MSC/$CD34^+$ seeded grafts 4 wk postaugmentation contained ~1.5 times and 2.75 times the number of vessels per square millimeter compared with $CD34^+$- and MSC-seeded grafts (230 ± 11.4 vs. 147.8 ± 11.0 and 83.4 ± 15.8, respectively). Similar trends were seen in PC (269 ± 19.8 vs. 184.4 ± 9.3 and 85.4 ± 4.4, respectively) and PSB (255.7 ± 10.2 vs. 170.4 ± 7.8 and 88.7 ± 3.4, respectively). Data for MSC-seeded grafts at the 10-wk time point are similar to MSC data at the 4-wk time point with regard to vessels per square millimeter. Data are summarized in Table S3 and is shown as means ± SE; $*P < 0.01$, $***P \leq 0.0001$ for MSC/$CD34^+$ vs. MSC and $CD34^+$ groups (4 wk).